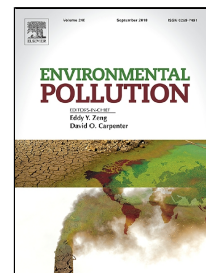# Accepted Manuscript

Synthesis of S-ligand tethered cellulose nanofibers for efficient removal of Pb(II) and Cd(II) ions from synthetic and industrial wastewater

Emmanuel Abu-Danso, Sirpa Peräniemi, Tiina Leiviskä, Amit Bhatnagar

1   **Synthesis of S-ligand tethered cellulose nanofibers for efficient removal of Pb(II) and**

2   **Cd(II) ions from synthetic and industrial wastewater**

3

4

5

6

7   **Emmanuel Abu-Danso[*,1], Sirpa Peräniemi[2], Tiina Leiviskä[3], Amit Bhatnagar[1]**

8

9

10

11   *[1]Department of Environmental and Biological Sciences, University of Eastern Finland,*
12   *FI-70211, Kuopio, Finland*
13

14   *[2]School of Pharmacy, University of Eastern Finland, FI-70211 Kuopio, Finland*

15

16   *[3]Chemical Process Engineering, University of Oulu, P. O. Box 4300, FI- 90014 Oulu*
17   *Finland*

18

19

20

21

22

23

24

25

26

27

28   *[*]**Corresponding author:** emmanuel.abu-danso@uef.fi

29

Abstract

Cellulose nanofibers (CNFs) tethered with sulphur as anionic ligand were synthesized from medical absorbent cotton by dissolution with NaOH, $CO(NH_2)_2$ followed by mechanical intrusion of sulphur from $SC(NH_2)_2$ at an elevated temperature. The solid-phase CNFs embedded with sulphur complexes possessed negative sites which were used to remove cationic metals viz., Pb(II) and Cd(II) from synthetic and industrial wastewater. The physicochemical properties of the CNFs were analyzed by Fourier transform infrared (FT-IR) spectroscopy, scanning electron microscopy (SEM), pH point of zero charge (pH_{pzc}) and X-ray photoelectron spectroscopy (XPS). Batch adsorption studies were conducted with synthetic wastewater to optimize the conditions for Pb(II) and Cd(II) removal by CNFs. Different adsorption kinetic models were applied to assess and define the adsorption mechanism. The maximum Langmuir adsorption capacity was found to be 1.16 and 0.82 mmol g^{-1} for Pb(II) and Cd(II) ions, respectively. Regeneration studies showed that the CNFs can be reused using 0.1 M NaOH as eluent. The percentage removal efficiency of different cationic metals by CNFs from untreated industrial wastewater ranged from ca. 90 to 98%.

In this work, anionic sulphur tethered cellulose nanofibers were synthesized from absorbent cotton and used in the removal of cationic metals from synthetic and industrial wastewater.

Keywords: Cellulose nanofibers; sulphur ligand; adsorption; lead; cadmium; modeling.

1. Introduction

Heavy metals emanate from anthropogenic activities such as mining, smelters and refineries (Järup, 2003), natural processes such as weathering of heavy metal-bearing rocks, volcanic emissions and biological activities (Huang et al., 2011). The exposure routes include air, water, and food (Guagliardi et al., 2012), which are essential human needs. Heavy metals have been designated as highly toxic, non-biodegradable and cumulative poison (WHO, 2011) and studies detailing these deleterious effects are well documented. To reduce the harmful effects of metals pollution, strict permissible levels of metals in drinking water are enforced by environmental protection agencies for example, 0.005 mg L^{-1} for cadmium Cd(II)) and 0.01 mg L^{-1} for lead Pb(II)) (WHO, 2008). Removal of heavy metals from water is necessary before discharging it to the environment. To remove heavy metals, various techniques including oxidative processes (Gihring et al., 2001), sorption (Manning and Goldberg, 1997), electrokinetic methods (Isosaari and Sillanpää, 2012) and membrane filtration (Kikuchi and Tanaka, 2012) have been used. These processes are, however, less efficient or can produce excess sludge (Kim and Benjamin, 2004).

In contrast, adsorption process for heavy metals removal is an economical and efficient approach and also has the advantage of possible regeneration (Bhatnagar et al., 2012). Different types of adsorbents have been studied for heavy metals remediation in water and search is still ongoing. To find an efficient biomaterial for metals adsorption, varied sources including lignin-containing agricultural waste such as wheat straw, rice bran, wood sawdust, pineapple peel have been used (Ghasemi et al., 2014). The use of cellulose as a biosorbent is often inhibited by the existence of strong inter and intra molecular network of hydrogen bonds which limits its ability to adsorb metal ions (Qin et al., 2016). For this reason, cellulose has generally been used as a composite or biofillers (de Oliveira Barud, Hélida Gomes et al., 2016) or modified to induce cationic exchange capacity (CEC) and increase

79   their metal ion adsorption capacities (Singha and Guleria, 2014). The modification

80   processes usually change cellulose to a reactive form by interfering with the H-bonds

81   (Bhattacharya and Misra, 2004). These modifications are expensive, complex and time

82   consuming (Qin et al., 2016) and usually require organic solvents. The current shift towards

83   green economy and the intense interest in materials prepared by simple method using cheap

84   readily available biomaterials with no or less detrimental derivatives is today's need.

85   This study aimed to synthesize novel S-ligand tethered cellulose nanofibers (CNFs) by

86   mechanical intrusion of sulphur (S)-radical after polymerization reduction using medical

87   absorbent cotton (as a cellulose source). The synthesized materials were used for the

88   removal of Pb(II) and Cd(II) and other cationic metals from synthetic and untreated

89   industrial wastewater. The tethered s-radical complexes were expected to enhance the

90   adsorption of cationic metals (Pb(II) and Cd(II)) due to negative ionic characteristics,

91   possessed by the adsorbent. The physico-chemical properties of prepared adsorbent were

92   analyzed by various techniques such as Fourier transformed infra-red spectroscopy (FT-IR),

93   scanning electron microscopy (SEM), pH at point of zero charge (pHzpc) and X-ray

94   photoelectron spectroscopy (XPS). The adsorption of Pb(II) and Cd(II) onto the synthesized

95   CNFs from synthetic wastewater was studied using different parameters including solution

96   pH, adsorbent dosage, contact time, initial adsorbate concentration, temperature and ionic

97   strength. The metal ions removal mechanisms were assessed by studying different kinetic

98   and isotherm models.

99

100 **2. Materials and methods**

101 *2.1. Chemicals*

102 Absorbent cotton was purchased from a local pharmacy shop in Kuopio, Finland. Cadmium

103 nitrate ($Cd(NO_3)_2 \cdot 4H_2O$), toluene and lead nitrate ($Pb(NO_3)_2$) were purchased from Sigma-

104   Aldrich, (Germany). Altia Oyj, (Finland) supplied ethanol. Sodium hydroxide was

105   purchased from Fisher scientific (UK). Thiourea and urea were supplied by Merck-

106   Schuchardt, (Germany). All stock solutions were prepared in milli-Q water. Untreated

107   industrial wastewater was obtained from local metal coating industry and mining seep water.

108   ## 2.2. Preparation of cellulose nanofibers (CNFs)

109   ### 2.2.1. Dewaxing pretreatment

110   The dewaxing procedure on absorbent cotton was conducted using soxhlet extraction at (90–

111   100∘C) in a mixture of toluene and ethanol (2:1 v/v) for 6 h. The dewaxed cotton was washed

112   in ethanol and dried in an oven (Memmert 100–800, Schwabach-Germany) at 80 °C to

113   constant weight. The dewaxing process removed residual wax for unimpeded dissolution of

114   the cotton fibers.

115   ### 2.2.2. Dissolution and sulphur complexes intrusion processes

116   The dissolution and reduction of degree of polymerization by alkali oxidation procedure and

117   subsequent sulphur (S) radical tethering was done by following modified procedures

118   reported elsewhere (Abu-Danso et al., 2017;Haskins and Hogsed, 1950). Briefly, a solution

119   containing 2.3 M NaOH, 1.8 M $CO(NH_2)_2$ and 1.75 M $SC(NH_2)_2$ as sulphur source was

120   cooled to ca. -3 °C. The dewaxed cotton (ca. 3.0 g) was dissolved in the solution to form a

121   cellulose gel. The NaOH served to disrupt the polymerization of the cellulose to shorter

122   chain for easy functionalization. The $CO(NH_2)_2$ functioned as the organogelator to tether

123   the sulphur complexes to the open-ended cellulose chain. This enabled formation of sulphur

124   substituted complexes and activated the cationic exchange capacity of CNFs at ca. -3 ^{0}C. To

125   complete the mechanical intrusion of sulphur complexes, the cellulose gel was spun with a

126   stirrer at 150 rpm for 30 min. The cellulose gel was centrifuged (Biofuge Stratos Heraeus

127   Intruments, kendro Lab., Germany) at 8000 rpm for 5 min to settle the cellulose and to

128 remove excess dissolution agents. The gel was then frozen in a refrigerator and freeze dried

129 (Christ Alpha 1-2, Biotech, Germany) for 120 h and pulverized.

130

131 ### *2.3. Characterization of CNFs*

132 ### *2.3.1. Fourier transform infrared spectroscopy (FT-IR)*

133 Changes in the functional groups on the surface of the synthesized CNFs, before and after

134 metals adsorption were analyzed using Fourier transform infrared spectroscopy (FT-IR)

135 with Thermo Nicolet Nexus 8700 model (Thermo electron, Madison USA) from 400–4000

136 cm^{-1} at 64 scans. The CNFs used for this analysis were thoroughly dried. The instrument

137 was cooled with liquid nitrogen and measurements were done using the MCT-B detector.

138 ### *2.3.2. Scanning electron microscopy (SEM)*

139 The surface morphology of the synthesized CNFs was analyzed by using Zeiss sigma HDVP

140 (Carl Zeiss GmbH, Oberkochen Germany) at different magnifications at 3 Kv. The CNFs

141 were sputter-coated using agar auto sputter to prevent interaction between CNFs powder

142 and the focused electron beam.

143 ### *2.3.3. X-ray photoelectron spectroscopy (XPS)*

144 The surface state of the CNFs before and after metals ions adsorption was evaluated using

145 XPS. The CNFs after the metals adsorption were centrifuged to aggregate the adsorbent and

146 dried in the oven (air circulating) at 30 ^{o}C for 6 h. The XPS spectra were carried out with a

147 Thermo Fisher Scientific ESCALAB 250Xi using a monochromatic Al Kα source (1486.6

148 eV) and an indium foil was used as the sample platform. The spectra for wide scan were

149 collected at each 1 eV and a pass energy of 150 eV. The high resolution spectra were

150 recorded with steps of 0.1 eV and a pass energy of 20 eV. The obtained data was analyzed

151 with Avantage Software and the background correction was done using Shirley function.

152 The charge correction was performed by setting the binding energy (BE) of adventitious

153 carbon to 284.8 eV. The high resolution spectra were fitted using the Shirley background

154 and the Gaussian-Lorentzian sum function.

2.3.4. Point of zero charge analysis

156 To determine the point of zero charge (pH_{PZC}) of the synthesized CNFs, 25 ml of 0.01 M

157 NaCl solution was taken in different tubes. The initial pH (pH_i) of the solutions in the tubes

158 was adjusted from 2-10 using 0.1 M NaOH or HCl. To each of the solution, 0.005 g of CNFs

159 was added and the solution was agitated at 80 rpm on a shaker for 24 h. The mixture was

160 filtered and the final pH (pH_f) was measured. The plot of pH_i against change in pH (ΔpH)

161 was used to deduce the point of zero charge (pH_{PZC}) of the CNFs following the procedure

162 as reported elsewhere (Tangsir et al., 2016).

2.4. Batch adsorption studies with synthetic wastewater

164 Solutions (200 mg L^{-1}) of the adsorbates viz. Pb(II) and Cd(II) were prepared and diluted

165 later to prepare the solutions of desired metal ions concentrations for the experiments. Batch

166 adsorption experiments were performed with CNFs to study the Pb(II) and Cd(II) adsorption

167 by CNFs. Adsorption kinetic experiments were carried out by adding a known amount of

168 CNFs in 15 mL capped tubes containing 50 mg L^{-1} of Pb(II) or Cd(II) ions solution. The

169 mixture was placed on a shaker and agitated at 80 rpm at room temperature to equilibrium.

170 After equilibration time, cellulose acetate membrane filters (pore size 0.45 μm, Sartorius,

171 Gmbh Germany) were used as a filter to separate the mixture and filtrate was analyzed for

172 residual Pb(II) or Cd(II) ions concentration using Atomic Absorption Spectroscopy (AAS)

173 (PerkinElmer Analytik Jena Zeenit 700, Jena, Germany). The amount of metal ions

174 adsorbed onto the CNFs was determined using eq. (1):

175 $$q_e = \frac{(C_e - C_i) * V}{m}$$ (1)   where q_e =

176 adsorption capacity of adsorbent (mg g^{-1})

177   C_i = initial concentration of metal ions (mg L^{-1})

178

179   C_e = equilibrium concentration of metal ions (mg L^{-1})

180

181   V = volume of the metal ion solution (L)

182

183   m = weight of CNFs (g)

184

185 Percentage removal (R%) was calculated from eq. (2):

186 $$(R\% \; removal) = \frac{C_i - C_e}{C_i} \times 100$$ (2)

187

188 *2.5 Adsorption studies with industrial wastewater*

189 Industrial wastewater was obtained from metal coating (EPW) and mining industry (MSW)

190 and characterized for conductivity and pH. The concentration of metal ions, that were

191 present in the wastewater from both industries, was measured by total reflection X-ray

192 fluorescence spectroscopy (TXRF) (Bruker Nano GmbH, Berlin, Germany). Lead and

193 cadmium mining industries generate between 200 – 500 mg L^{-1} concentration of the metals

194 in their wastewater as reported in other study (Ucun et al., 2003). To assess the applicability

195 of the CNFs in industrial wastewater with high concentrations of the metals, the obtained

196 industrial wastewater was divided into two parts. One part of the obtained wastewater was

197 spiked with different concentrations of Pb(II) and Cd(II) viz. 200, 300 and, 400 mg L^{-1} to

198 increase their levels to the levels mining industries generate. The adsorption studies were

199 subsequently conducted as described in section 2.4. The residual Pb(II) and Cd(II) ions were

200 analyzed using AAS due to the high concentration of the metal ions.

201 The other part of the wastewater (as received and no spiking of Pb(II) and Cd(II) ions) was

202 used for the adsorption studies using CNFs. The residual metal ions (Zn, Hg, Co, Mn, Ba,

203 Ni and Ba) were analyzed using Inductively coupled plasma mass spectrometry (ICP-MS)

204 (PerkinElmer Analytik Jena Zeenit 700, Jena, Germany). The ICP-MS was used in this

205 analysis due to high sensitivity for low concentration of metal ions and the ability to analyze

206 a selected spectrum of metals with a good accuracy.

207

3. Results and discussion

3.1. Characterization

3.1.1. Point of zero charge analysis

211 The pH_{PZC} measurements for the CNFs at different pH scales exhibited different net proton

212 charge as shown in (**Fig. 1 a)**. Changes in initial pH from 2 to 10 resulted in a general

213 decrease in acidity of the medium which also resulted in decreasing negativity. However,

214 the decreasing negative charge was not low enough to reach a positive value hence, iso-

215 electric point could not be obtained thereby, making the CNFs surface negative in the pH

216 range of 2 to 10. This was in agreement with previous report of zeta potential measurements

217 (Abu-Danso et al., 2017).

3.1.2 Fourier transform infrared spectroscopy (FT-IR)

219 The FT-IR spectra of CNFs before and after Pb(II) and Cd(II) adsorption are shown in (**Fig.**

220 **1 b).** The differences in the peaks between the synthesized S-tethered CNFs, and CNFs after

221 Cd(II) and Pb(II) adsorption indicated the presence of metal ions on the surface of the CNFs,

222 which is indicated by shifts in the peaks of functional groups of the parent CNFs. This

223 phenomena of masking or distortion of functional groups is in agreement with studies

224 reported elsewhere (Parsons et al., 2013). The observed differences in the spectra include

225 the absence of peaks at 2094 cm^{-1} (-N-C-S intense), 1122 cm^{-1} (C-OCN stretch), 1594 cm^{-1}

226 (-NH primary bend), and 781 cm^{-1} (-CH$_2$-S- thioethers stretch) in both Cd(II) and Pb(II)

227 laden CNFs spectra. The diminished N-H stretch at 3443 cm^{-1} in the spectra after Cd(II) and

228 Pb(II) adsorption also suggests some interactions between the metals and the N-H group

229 since N-H is known to have chelating capabilities. The disappearance or diminishing of

230 peaks in the Pb(II) and Cd(II) laden CNFs clearly suggest that the -S- groups interacted with

231 the metals on the surface of CNFs. This mechanism of interaction between adsorbates and

232 adsorbent surface is in agreement with other study (Wang et al., 2017). On the contrary,

233 bands in the region of 3200 - 3300 cm^{-1} and 1300 - 1450 cm^{-1}, which are indicative of -OH

234 group stretch and -OH in plane bend, were present on the Pb(II) and Cd(II) laden CNF,

235 which suggests that the -OH groups had no influence in the adsorption of these metals.

236 *3.1.3. Scanning electron microscopy (SEM)*

237 The SEM images taken at magnifications (17 and 15 Kx) are shown in **Fig. 1 c** and **d**. **Fig.**

238 **1 c** shows the mesh-like structure of the CNFs due to the freeze-drying process and treatment

239 agents used while **Fig. 1 d** shows the porosity of the material upon drying. The analysis

240 showed a complete disappearance of the cotton strands to form uniform cellulose which

241 proves that the dissolution procedure used was successful. The BET and crystalline size

242 distribution analyses of the CNFs have been previously reported (Abu-Danso et al., 2017).

3.1.4. X-ray photoelectron spectroscopy (XPS)

3.1.4.1. Scans spectra of CNFs

The XPS scans of CNFs are represented in **Fig. 1 e-i**. The wide scan (**Fig. 1 e**) indicated the presence of C and O which are found around binding energies of 284 and 530 eV (Ishimaru et al., 2007;Monier et al., 2014) and typical of cellulose. The wide scan also revealed the presence of N, Na, and S as a result of the synthesis process. The C 1s spectra (**Fig. 1 f**) was fitted to four peaks corresponding to carbon atoms in different chemical environments; the C-C, C-H; 284.8 eV is the characteristic of cellulose (Yu et al., 2013), C-O, C-S, C-N; 286.5 - 286.6 eV, O-C-O, C=O, N-C=S; 288 eV and the carboxylate group (O-C=O; 289.0-289.6 eV).

The S 2p, O 1s and N 1s spectra are presented in **Fig. 1 g-i**. The $CO(NH_2)_2$, and $SC(NH_2)_2$ derivatives are indicated on the N 1s and S 2p spectra. The N 1s on the wide scan present in 402.3 eV is in agreement with other study (Monier et al., 2014). The N 1s fitting revealed a peak at 399.6 eV, indicative of nitrogen atoms in $-NH_2-$ functional groups, is in agreement with (Lindberg et al., 1970;Li et al., 2016). The other peak at the lower binding energy (398.2 eV) could be attributed to -NH- shifted to lower binding energy at equilibrium which is a known behaviour of carbonyl of a keto form (Haushalter et al., 1996). The presence of S is indicated by S 2p at 168 eV (Monier et al., 2014;Li et al., 2016). The S fittings in **Fig. 1 g** showed 3 peaks. Two of the sulphur components appear to have discharged in a ratio close to 1:1 at binding energies 162.0 eV (indicative of thiourea) and 168.2 eV although the spectra showed a bridge between the S components. The spectra also showed two other disproportionate sulphur as also reported (Lindberg et al., 1970;Liang et al., 2015). According to (Lindberg et al., 1970), the disproportionality of the sulphurs suggests a yield of unstable components which can also cause shifts in the peak. The S $2p_{3/2}$ peak around

267 166.5 eV is representative of sulphur complexes and thiosulphate at 168.2 eV (Lindberg et

268 al., 1970;Li et al., 2016). The O 1s spectrum was fitted with two components (**Fig. 1 h**). The

269 larger component is mainly O bonded to C around 531.3 eV, which is consistent with other

270 study (Li et al., 2016). The smaller component at 532.7 is absorbed water (-OH) (Li et al.,

271 2016) as a result of the CNFs synthesis procedure.

272 *3.1.4.2. Elemental content of CNFs before and after sorption*

273 The surface elemental composition of CNFs was analyzed and it showed a composition of

274 the materials, involved in the synthesis process (**Fig. 1 j**). The XPS surface elemental

275 analyses of the CNFs after adsorption of Cd(II) and Pb(II) also revealed a composition

276 which included the adsorbed metals, as shown in **Fig. 1 j**. The CNFs revealed the presence

277 of O, C, N, Na and S elements which are typical of cellulose treated with the combination

278 of dissolution agents used in this study.

279 *3.2. Batch adsorption experiments*

280 *3.2.1. Effect of solution pH*

281 The solution pH in an adsorption process, influence the adsorption capacity of an adsorbent

282 since the type of surface charges, possessed by the adsorbents and the adsorbate's ionic

283 character affects adsorption of metal ions. The effect of pH on the adsorption of Pb(II) and

284 Cd(II) is shown in **Fig. 2 a**. The adsorption of Cd(II) and Pb(II) was found to increase with

285 increasing pH which can be attributed to the changes in surface charge of CNFs under

286 different pHs and the chelating properties of the CNFs. At low pH, more H^+ ions were

287 present in the solution and therefore, repulsion between the cationic metal ions and the H^+

288 might have contributed to the low adsorption capacity of the CNFs which is also reported

289 in other studies (Navarro et al., 1996;Qin et al., 2016). With increasing pH, H^+ ions are

290 available in less amount and the surface of the CNFs became mostly negative and as a result,

291 metal ions were adsorbed in higher amount due to electrostatic attraction (Qin et al., 2016).

292 Overall, the capacity of CNFs to adsorb Pb(II) was higher than Cd(II).

3.2.2. Effect of adsorbent dosage

294 The adsorption of Pb(II) and Cd(II) by different dosages of CNFs was studied and the results

295 are shown in **Fig. 2 b**. The CNFs dosage was changed starting from 0.2 g L^{-1} to 1.6 g L^{-1}

296 and the trend of the results were similar for both Pb(II) and Cd(II). The highest removal

297 efficiency was recorded with the highest adsorbent dosage. This phenomenon is attributed

298 to increased availability of active sites with a higher adsorbent dose and hence, removal

299 capacity increased from 52 to ca. 99% and 48 to ca. 97% for Pb(II) and Cd(II) ions,

300 respectively. In contrast, a lower adsorbent dose provided less adsorption sites leading to

301 the less adsorption and therefore, a low removal capacity was observed.

3.2.3. Effect of temperature

303 Adsorption experiments were also conducted at 35 and 45 °C besides room temperature to

304 study the effect of temperature on the adsorption of Pb(II) and Cd(II) by CNFs, as shown in

305 **Fig. 2 c**. The results showed that adsorption capacity was slightly lower at room temperature

306 (ca. 25 °C). The other studied temperatures (viz. 35 and 45 °C) did not show a remarkable

307 difference in the adsorption of both Pb(II) and Cd(II) ions. This negligible effect of different

308 temperature on adsorption capacity has been reported by (Bhatnagar et al., 2009) with wider

309 temperature ranges.

3.2.3.1. Thermodynamic parameters

311 The enthalpy change ($\Delta H°$) and entropy ($\Delta S°$) values for the thermodynamics of the

312 adsorption of Pb(II) and Cd(II) ions by the synthesized CNFs were obtained from the slope

313   and the intercept of the plot of ln K_0 vs 1/T. The Gibbs free energy (ΔG°) was calculated by

314   using eq. (3): (Anastopoulos and Kyzas, 2016)

315    $$\Delta G° = - RTln (KM_{adsorbate} * 55.5) \tag{3}$$

316   where R is the gas constant (8.314 J mol^{-1} K), T represents absolute temperature (K), K (L

317   g^{-1}) represents thermodynamic equilibrium of Langmuir constant, M is molecular weight of

318   adsorbent and 55.5 is water concentration. The change in free energy of the system was

319   determined from eq. (4):

320    $$\ln (K_o) = - \left(\frac{\Delta H°}{RT} + \frac{\Delta S°}{R} \right) \tag{4}$$

321   The values of enthalpy change (ΔH°) and Gibb's free energy (ΔG°) for both metals, Pb(II)

322   and Cd(II) are presented in **Table 1**. The positive value of the standard enthalpy suggests

323   that the adsorption of Pb(II) and Cd(II) by CNFs is an endothermic process.

324   The negative value of Gibb's free energy also suggests that the adsorption process for Pb(II)

325   and Cd(II) was a spontaneous process (Chella et al., 2015). The positive values obtained for

326   ΔS° indicates an increase in the randomness of the attachment of the metal ions at the solid-

327   liquid interface of CNFs as reported elsewhere (Anastopoulos et al., 2013).

328   *3.2.4. Effect of ionic strength*

329   One important parameter in adsorption studies is the effect of the presence of salt (NaCl) in

330   wastewater. The existence of high ionic strength can interfere with the adsorption processes

331   (Xu et al., 2011). The sorption capacity of CNFs for Pb(II) and Cd(II) metal ions in the

332   presence of different concentrations of salt is presented in **Fig. 2 d**.

333   The NaCl concentrations were taken as 1.0 – 4.0 M in the studies with Pb(II) adsorption and

334   0.5 – 3.0 M in the studies with Cd(II) adsorption. From **Fig. 2 d**, it can be seen that the

335   adsorption capacity of CNFs for Pb(II) ions decreased from ca. 86 mg g^{-1} (0.41 mmol g^{-1})

336   to ca. 25 mg g^{-1} (0.12 mmol g^{-1}) when the concentration of NaCl was increased from 1.0 M

337   to 4.0 M. The adsorption capacity of CNFs for Cd(II) ions decreased from ca. 30 mg g^{-1}

338   (0.266 mmol g^{-1}) to 2 mg g^{-1} (0.017 mmol g^{-1}) in the presence of 0.5 M to 2.0 M NaCl. The

339   CNFs showed no capacity to adsorb Cd(II) ions in the presence of 3 M NaCl as shown in

340   **Fig. 2 d**. This adsorption behavior could be as a result of competition between Na$^+$ ions with

341   Pb(II) or Cd(II) ions for the same binding sites. Since the adsorption process has been

342   considered to be monolayer, the sites for other ions (Pb(II) and Cd(II)) decreased due to the

343   presence of Na$^+$ ions, resulting in lower uptake of the target metal ions. The trend of

344   decreasing adsorption capacity was gradual towards Pb(II) ions and steep towards Cd(II)

345   ions.

3.2.5. Effect of contact time and adsorption kinetics

347   The adsorption kinetics of Pb(II) and Cd(II) by CNFs is represented in **Fig. 3 a and b**. The

348   results showed a similar trend for both metal ions. Adsorption was found to increase rapidly

349   initially from 0 to ca. 40 min. and subsequently stabilized after ca. 60 min. indicating that

350   equilibrium was achieved. The average adsorption capacity after equilibration was found to

351   be ca. 123.78 mg g^{-1} (0.598 mmol g^{-1}) for Pb(II) and ca. 57.97 mg g^{-1} (0.515 mmol g^{-1}) for

352   Cd(II), respectively. This greater affinity of Pb(II) ions to the binding sites of the CNFs

353   compared to the Cd(II) ions has already been discussed in the results of the pH studies.

354   The adsorption kinetics was assessed with different kinetic models. The pseudo-first order

355   model can be given by eq. (5) (Lagergren, 1898):

356    $$q_t = q_e \left(1 - e^{-k_{1t}}\right) \tag{5}$$

357   where q_e and q_t represent the amount of metals adsorbed (mg g^{-1}) at equilibrium and time t

358   (min) while k_1 represents pseudo-first order (min^{-1}) rate constant.

359   Pseudo-second order model assumes a chemical rate determining step and can be written as

360   follows (Ho and McKay, 1999):

361     $$q_t = \frac{k_2 q_e^2 t}{1 + k_2 q_e t} \qquad (6)$$

362   where k_2 is the pseudo-second order rate (g mg^{-1} min^{-1}) constant.

363   Avrami model (Avrami, 1939) can be given as follows:

364     $$q_t = q_e \left(1 - e^{\left(- (k_{av} t)^n \right)} \right) \qquad (7)$$

365   where K_{AV} (min^{-1}) is the Avrami constant.

366   The values of model parameters are summarized in **Table 2**. Based on the results, it was

367   found that pseudo-second order model best describes the adsorption process compared to

368   the other models, as shown from the correlation coefficients (R^2).

369   Besides correlation coefficients (R^2), the calculated adsorption capacities, $q_{e(cal)}$, are also

370   closer to those determined by experiments, $q_{e(exp)}$, in case of pseudo-second-order model,

371   indicating that the adsorption kinetics of Pb(II) and Cd(II) on CNFs can be better described

372   by pseudo-second-order model.

373   The intra-particle diffusion model was also applied to determine the rate-limiting step

374   (Weber and Morris, 1963) can be given as:

375     $$q_t = k_p t^{\frac{1}{2}} + c \qquad (8)$$

376 where k_p represents intra-particle diffusion rate constant (mg g^{-1} min $^{-1/2}$) and C (mg g^{-1}) is

377 the intercept which measures the thickness of the boundary layer over which the diffusion

378 occurs. The Weber and Morris plots of Pb(II) and Cd(II) adsorption (**Fig. 3 c**) showed two

379 different phases. The first phase is attributed to the immediate utilization of the most readily

380 available adsorbing sites on the adsorbent surface. Second phase may be attributed to very

381 slow diffusion of the adsorbate from the surface site into the inner pores.

382 *3.2.6. Adsorption isotherms*

383 To study the relationship between the concentration of the metal ions in liquid phase and

384 the amount that can be adsorbed by the adsorbent at equilibrium, different adsorption

385 isotherm models were studied. The equilibrium adsorption by the synthesized CNFs was

386 studied as a function of Pb(II) and Cd(II) ions concentration and the experimental data were

387 fitted to four isotherm models. The Langmuir model describes an adsorption process based

388 as a monolayer surface adsorption in which ions/molecules of identical energy occupy

389 definite localized sites (homogenous) on the surface involved (Langmuir, 1918). The

390 strictness of the Langmuir model means that the localized ion has no lateral interactions

391 between the adsorbed ions even on the adjacent sites and the localization will proceed to a

392 plateau exponentially until no further adsorption as reported by (Langmuir, 1918).

393 The Langmuir model can be given by eq. (9):

$$ 394 \quad q_e = \frac{q_m K_L C_e}{1 + K_L C_e} \qquad\qquad (9) $$

395 where q_e (mg g^{-1}) is the amount of adsorbate adsorbed by the synthesized CNFs at

396 equilibrium time, C_e represents adsorbate concentration at equilibrium time (mg L^{-1}), q_m (mg

397 g^{-1}) represents maximum monolayer adsorption capacity and K_L is the Langmuir constant

398 (L mg^{-1}).

399   The Freundlich model assumes a heterogeneous surface and a multilayer adsorption and

400   predicts a non-uniform surface attachment using energy to drive the distribution of the ions

401   (Freundlich, 1906).

402   The Freundlich model is described by the following equation:

403   $$q_e = K_F C_e^{1/n} \qquad (10)$$

404   where K_F and n are constants for a given adsorbent – adsorbate system.

405   The Sips model is a three parameter model and combines the features of Langmuir and

406   Freundlich models (Sips, 1948).

407   The Sips model can be described by eq. (11):

408   $$q_e = \frac{q_{m(K_s C_e)^m}}{1 + (K_s C_e)^m} \qquad (11)$$

409   where K_S (L mg^{-1}) is the Sips affinity constant.

410   The Redlich-Peterson model is also a three parameter model that predicts both homogenous

411   and heterogeneous systems (Redlich and Peterson, 1959).

412   $$q_e = \frac{K_{RP} C_e}{1 + a_{RP} C_E^{\beta}} \qquad (12)$$

413   K_{RP} (L g^{-1}) and a_{RP} (L mg^{-1}) are Redlich-Peterson constants.

414   The fitting of the data into different adsorption isotherm models is presented in **Fig. 3 d and**

415   **e**. The Langmuir model fitted better with the adsorption data of the two metal ions as shown

416   by good correlation coefficients (Pb(II): 0.999, and Cd(II): 0.999) compared with the other

417   models (**Table 2**) and thus, suggesting a monolayer adsorption during the process. The

418   theoretical maximum adsorption capacity was calculated as 239.64 mg g^{-1} (1.160 mmol g$^-$

419 ^{1}) and 92.32 mg g^{-1} (0.821 mmol g^{-1}) for Pb(II) and Cd(II), respectively. To check the

420 favorability of the adsorption process, the separation factor (R$_L$) was used by (Weber and

421 Chakravorti, 1974) calculated from eq. (13):

422 $$R_L = \frac{1}{1 + C_o K_L} \qquad (13)$$

423 where R$_L$ is a dimensionless equilibrium parameter or the separation factor and C$_0$ is the

424 initial concentration of metal ions (mg L^{-1}). The adsorption process is favorable if (0 < R$_L$

425 < 1), and unfavorable if (R$_L$ > 1). The results of this study showed that the adsorption of

426 Pb(II) and Cd(II) metal ions by the synthesized CNFs is a favorable one since the R$_L$ value

427 for both metal ions was between 0 and 1 (**Table 2**).

428 Generally, adsorption capacity of CNFs for Pb(II) ions was higher compared to Cd(II) ions.

429 This high affinity for Pb(II) ions by CNFs over Cd(II) ions could possibly be as a result of

430 the characteristics of Pb(II) ions, summarized in **Table 3** and also reported elsewhere

431 (Hossain et al., 2014). The higher removal efficiency of CNFs for Pb(II) as compared to

432 Cd(II) can be explained considering the binding strength of the metal ions. Pb(II) and Cd(II)

433 share features of both hard and soft ions and are termed as borderline ions. With soft donors

434 like N, S, P, and As, soft cations form more stable complexes. Hard ions have the tendency

435 to form strong bonds with highly electronegative donors (Dean, 1990). Hard ions also form

436 ionic bonding to most extent. On the contrary, soft ions form covalent bonding wherein free

437 energy is enthalpic in nature (Nieboer and McBryde, 1973). The important binding strength

438 parameters of the two studied metals are presented in **Table 3**. The ionic bond strength of

439 Pb(II) is greater than Cd(II) which is revealed by the (z^2 / r_{hyd}) criterion (**Table 3**). The

440 parameter $X_m^2 \left(r_{cryst} + 0.85 \right)$, introduced by Nieboer and McBryde (Nieboer and McBryde,

441 1973), is a measure for the strength of covalent bonding. The contribution of N or O donors

442 to the bond distance is given by the factor '0.85'. Soft ions are characterized by

443 $X_m^2\left(r_{cryst}+0.85\right)>7$ and hard ions have $X_m^2\left(r_{cryst}+0.85\right)<\approx4.2$. The relative contribution

444 of covalent bonding follows the order, Pb(II) > Cd(II), which is confirmed by

445 $X_m^2\left(r_{cryst}+0.85\right)$ criterion. The total binding strength (ξ) is higher for Pb(II) than Cd(II)

446 (**Table 3**) which explains higher Pb(II) binding to CNFs as compared to Cd(II).

447 Furthermore, Pb(II) has a higher hydrolysis constant 43.61 (-log β pq) at room temperature

448 in aqueous medium compared to Cd(II) 32.37 (-log β pq) (Brown, 1984). Pb(II) has lower

449 enthalpy of fusion (5.121 kJ mol^{-1}) compared to Cd(II) (6.11 kJ mol^{-1}) (De Podesta, 2002)

450 and therefore, Pb(II) requires less energy to be adsorb. This characteristic can be attributed

451 to the higher adsorption of Pb(II) ions compared to Cd(II) as also reported by (Anastopoulos

452 et al., 2015).

3.2.7. Reusability of synthesized CNFs

454 The reusability of adsorbents is important in water treatment as it makes the process

455 economically feasible. To assess the reusability of synthesized CNFs, H_2O and 0.1 M NaOH

456 were chosen as the eluents. The results of 0.1 M NaOH as eluent are presented in **Fig. 3 f.**

457 The results showed that 0.1 M NaOH is a better eluent for the regeneration of CNFs. After

458 4 cycles, 0.1 M NaOH was still able to elute the Pb(II) and Cd(II) ions and the CNFs showed

459 consistent removal efficiency. The removal efficiency with H_2O as eluent for Pb(II) ions

460 decreased from 63.7 to 19.8% from the 1st to 4th cycle (results not shown). The removal

461 efficiency of Cd(II) however decreased significantly from 71.7 to 4.1% from the 1st to 2nd

462 cycle (results not shown). This elution phenomenon could be as a result of the feasibility of

463 the reaction; $Pb(NO_3)_2 + 2NaOH \rightarrow Pb(OH)_2 + 2NaNO_3$ compared to the feasibility of

464 $Pb(NO_3)_2 + H_2O_{temp} \rightarrow Pb(OH)NO_3 + HNO_3$ at room temperature. From the two equations,

465 the reaction of the Pb(II) ions with water requires heat to proceed. However, the elution

466 reaction proceeded at room temperature. This is likely to result in weak metal ion – H_2O

467 complexation to create free sites on the CNFs for repeated usage thereby making water a

468 poor eluent compared to NaOH. One other limitation of water as an eluent is from the self-

469 ionization reaction; $H_2O + H_2O \leftrightarrow H_3O^+ + OH^-$ characteristic in aqueous media as reported

470 by (Brown and Ekberg, 2016). The unstable hydoxonium cation (H_3O^+) interferes in the

471 elution of the metal ion by forming varied ionized forms of the metal and H^+ which can

472 attach to the adsorbent and prevent elution by the same water (Brown and Ekberg, 2016).

473 The percentage removal efficiency of CNFs for Pb(II) and Cd(II) metal ions was > 90 and

474 60%, respectively. The results herein indicate that the synthesized CNFs can be used

475 repeatedly to remove Pb(II) and Cd(II) metal ions using the adsorption and desorption

476 cycles.

477

478 **3.3. Application of CNFs for industrial wastewater treatment**

479 The CNFs herein synthesized were used as an adsorbent for the removal of different cationic

480 metal ions from real (untreated) metal coating and mining seep wastewater. The results

481 revealed that CNFs are effective in removing Pb(II) and Cd(II) from spiked wastewater

482 (**Table 4**). For the metal coating wastewater, the highest uptake capacities were found to be

483 890 mg g^{-1} (4.30 mmol g^{-1}) and 246.9 mg g^{-1} (2.20 mmol g^{-1}) for Pb(II) and Cd(II),

484 respectively by CNFs. For the mining seep wastewater, the highest uptake capacities were

485 observed as 782.49 mg g^{-1} (3.78 mmol g^{-1}) and 170.80 mg g^{-1} (1.52 mmol g^{-1}) for Pb(II) and

486 Cd(II), respectively (**Table 4**). The trend of these results was similar to the results with

487 synthetic water and the reason for this phenomenon has been explained in the previous

488 sections. Generally, the adsorption capacity increased when the metal concentration was

489 increased. However, there was a reverse of the trend in the adsorption of Cd(II) in the mining

490   seep wastewater where the uptake capacity reduced with a higher metal concentration as

491   shown in **Table 4.**

492   The results of the other wastewater which was studied without additional metal ion spiking

493   are also presented in **Table 4**. The results revealed that the removal efficiency of the metal

494   ions ranged from ca. 90 to 98%. The removal efficiency was however significantly low for

495   manganese (52.7%).

496

497   *3.4. Mechanism of metals adsorption by CNFs*

498   The XPS wide scan analysis of the synthesized CNFs after adsorption of Pb(II) and Cd(II)

499   is shown in **Fig. 4 a**. The analysis shows substituted Pb(II) and Cd(II) peaks compared with

500   XPS wide scan of CNFs (**Fig. 1 e).** The presence of these new peaks coincided with absence

501   or the suppression of S groups as also shown in the FT-IR analysis (**Fig**. **1 b)**. The high

502   resolution scan of Pb(II) 4f (**Fig. 4 b**) showed a doublet with Pb(II) $4f_{7/2}$ at 138.4 eV and the

503   high resolution scan of Cd(II) 3d (**Fig. 4 c**) showed a doublet Cd(II) $3d_{5/2}$ peak at 405.6 eV

504   and Cd(II) $3d_{3/2}$ peak at 412.4 eV confirming the accumulation of Pb(II) and Cd(II) ions on

505   the surface of the CNFs after adsorption. Furthermore, the S 2p peaks before adsorption of

506   metal ions at 162 eV reduced after adsorption as shown in **Fig. 4 d and e** suggesting

507   exchange of sulphur-complexes for the metal ions.

508   The proposed adsorption mechanism is presented in **Fig. 5.** which suggests that higher metal

509   ions-S-groups complexation takes place between metals and CNFs. This phenomenon might

510   be due to the capacity of S-ligand in $SC(NH_2)_2$ to interact easily with the Pb(II) and Cd(II)

511   ions which is aided by the diffuse electron cloud of $SC(NH_2)_2$ (Gregoret et al., 1991).

512   Furthermore, the head group orientation of $SC(NH_2)_2$ allows multiple interactions with

513   positive species within the bonding region. This is in contrast to one dimensional bonding

514 behavior of $CO(NH_2)_2$, as also reported in other studies (Wilson and Tarbell, 1950;Stefaniu

515 et al., 2015). This phenomenon favours sulphur-complexes-metal ions interactions

516 compared to $CO(NH_2)_2$. All these features of $SC(NH_2)_2$ might be responsible for the

517 adsorption of Pb(II) and Cd(II) by CNFs.

4. Conclusions

519 In this study, cellulose nanofibers (CNFs) tethered with sulphur as anionic ligand were

520 synthesized from medical absorbent cotton by dissolution with NaOH, organogelator

521 $CO(NH_2)_2$ followed by mechanical intrusion of sulphur from $SC(NH_2)_2$. The CNFs were

522 characterized by pH_{pzc}, FT-IR, SEM and XPS and used for the removal of Pb(II) and Cd(II)

523 and other metal ions from synthetic and untreated industrial wastewater. The experimental

524 data fitted well with Langmuir isotherm model. The maximum monolayer uptake capacity

525 was found to be 239.64 mg g^{-1} (1.160 mmol g^{-1}) and 92.32 mg g^{-1} (0.821 mmol g^{-1}) for

526 Pb(II) and Cd(II) ions, respectively. The adsorption kinetics was rapid and equilibrium was

527 reached in less than 1 h. The pseudo-second order kinetic model best described the metals

528 adsorption which suggests the adsorption process was a chemical process. Regeneration

529 studies showed that CNFs can be reused multiple times with 0.1 M NaOH as an eluent. The

530 synthesized CNFs removed ca. 90-98% of the metal ions present in industrial wastewater.

531 The prepared CNFs show promising results and suggest that the material can be used in

532 water treatment (cationic metals removal).

533

538 AAS analysis. Authors also thank Janne Immonen of Suomen Elektropinta, Kuopio for

539 providing untreated wastewater for the study. First author is grateful for the guidance from

540 lab colleague, Santhosh Chella (Post-doc), University of Eastern Finland.

541

542

543 **References**

544 Abu-Danso, E., Srivastava, V., Sillanpää, M., Bhatnagar, A., 2017. Pretreatment assisted
545 synthesis and characterization of cellulose nanocrystals and cellulose nanofibers from
546 absorbent cotton. Int. J. Biol. Macromol. 102, 248-257.

547 Anastopoulos, I., Massas, I., Ehaliotis, C., 2013. Composting improves biosorption of
548 Pb2 and Ni2 by renewable lignocellulosic materials. Characteristics and mechanisms
549 involved. Chem. Eng. J. 231, 245-254.

550 Anastopoulos, I., Massas, I., Ehaliotis, C., 2015. Use of residues and by-products of the
551 olive-oil production chain for the removal of pollutants from environmental media: A
552 review of batch biosorption approaches. Journal of Environmental Science and Health,
553 Part A 50, 677-718.

554 Anastopoulos, I., Kyzas, G. Z., 2016. Are the thermodynamic parameters correctly
555 estimated in liquid-phase adsorption phenomena? Journal of Molecular Liquids,
556 Elsevier, 218, 174-185.

557 Avrami, M., 1939. Kinetics of phase change. I General theory. J. Chem. Phys. 7, 1103-
558 1112.

559 Bhatnagar, A Choi, Y., Yoon, Y., Shin, Y., Jeon, B., Kang, J. 2009. Bromate removal
560 from water by granular ferric hydroxide (GFH) Journal of Hazard. Materials., 170, 1,
561 134- 140.

562 Bhatnagar, A., Vilar, V.J., Ferreira, C., Botelho, C.M., Boaventura, R.A., 2012.
563 Optimization of nickel biosorption by chemically modified brown macroalgae (Pelvetia
564 canaliculata). Chem. Eng. J. 193, 256-266.

565 Bhattacharya, A., Misra, B., 2004. Grafting: a versatile means to modify polymers:
566 techniques, factors and applications. Progress in polymer science 29, 767-814.

567 Brown, P.L., Ekberg, C., 2016. Hydrolysis of Metal Ions. John Wiley & Sons.

568 Brown, P.L., 1984. Studies on the hydrolysis of metal ions. Ph.D dissertation, University
569 of Wollongong, Wollongong , Australia.

Chella, S., Kollu, P., Komarala, E.V.P., Doshi, S., Saranya, M., Felix, S., Ramachandran, R., Saravanan, P., Koneru, V.L., Venugopal, V., 2015. Solvothermal synthesis of MnFe 2 O 4-graphene composite—Investigation of its adsorption and antimicrobial properties. Appl. Surf. Sci. 327, 27-36.

de Oliveira Barud, Hélida Gomes, da Silva, R.R., da Silva Barud, H., Tercjak, A., Gutierrez, J., Lustri, W.R., de Oliveira, O.B., Ribeiro, S.J., 2016. A multipurpose natural and renewable polymer in medical applications: Bacterial cellulose. Carbohydr. Polym. 153, 406-420.

De Podesta, M., 2002. Understanding the Properties of Matter. 2nd Edn, Taylor and Francis London, CRC Press CRC Press.

Dean, J., 1990. Lange's handbook of chemistry. Material and manufacturing process 5, 687-688.

Evans, H., 1995. Ionic radii in crystals. CRC handbook of chemistry and physics , 12-18.

Freundlich, H., 1906. Over the adsorption in solution. J. Phys. Chem. 57, 1100-1107.

Ghasemi, M., Naushad, M., Ghasemi, N., Khosravi-Fard, Y., 2014. Adsorption of Pb (II) from aqueous solution using new adsorbents prepared from agricultural waste: adsorption isotherm and kinetic studies. Journal of Industrial and Engineering Chemistry 20, 2193-2199.

Gihring, T.M., Druschel, G.K., McCleskey, R.B., Hamers, R.J., Banfield, J.F., 2001. Rapid arsenite oxidation by Thermus aquaticus and Thermus thermophilus: field and laboratory investigations. Environ. Sci. Technol. 35, 3857-3862.

Gregoret, L.M., Rader, S.D., Fletterick, R.J., Cohen, F.E., 1991. Hydrogen bonds involving sulfur atoms in proteins. Proteins: Structure, Function, and Bioinformatics 9, 99-107.

Guagliardi, I., Cicchella, D., De Rosa, R., 2012. A geostatistical approach to assess concentration and spatial distribution of heavy metals in urban soils. Water, Air, & Soil Pollution 223, 5983-5998.

Haskins, J., Hogsed, M., 1950. The alkaline oxidation of cellulose. I. Mechanism of the degradative oxidation of cellulose by hydrogen peroxide in presence of alkali. J. Org. Chem. 15, 1264-1274.

Haushalter, K.A., Lau, J., Roberts, J.D., 1996. An NMR Investigation of the Effect of Hydrogen Bonding on the Rates of Rotation about the C− N Bonds in Urea and Thiourea. J. Am. Chem. Soc. 118, 8891-8896.

Ho, Y., McKay, G., 1999. Pseudo-second order model for sorption processes. Process biochemistry 34, 451-465.

606 Hossain, M., Ngo, H., Guo, W., Nghiem, L., Hai, F., Vigneswaran, S., Nguyen, T., 2014.
607 Competitive adsorption of metals on cabbage waste from multi-metal solutions.
608 Bioresour. Technol. 160, 79-88.

609 Huang, X., Sillanpää, M., Gjessing, E., Peräniemi, S., Vogt, R., 2011. Water quality in
610 the southern Tibetan Plateau: chemical evaluation of the Yarlung Tsangpo
611 (Brahmaputra). River research and applications 27, 113-121.

612 Ishimaru, K., Hata, T., Bronsveld, P., Meier, D., Imamura, Y., 2007. Spectroscopic
613 analysis of carbonization behavior of wood, cellulose and lignin. J. Mater. Sci. 42, 122-
614 129.

615 Isosaari, P., Sillanpää, M., 2012. Effects of oxalate and phosphate on electrokinetic
616 removal of arsenic from mine tailings. Separation and purification technology 86, 26-
617 34.

618 Järup, L., 2003. Hazards of heavy metal contamination. Br. Med. Bull. 68, 167-182.

619 Kertes, A.S., Marcus, Y., 1969. Solvent Extraction Research: Proceedings. Wiley-
620 Interscience.

621 Kikuchi, T., Tanaka, S., 2012. Biological removal and recovery of toxic heavy metals
622 in water environment. Crit. Rev. Environ. Sci. Technol. 42, 1007-1057.

623 Kim, J., Benjamin, M.M., 2004. Modeling a novel ion exchange process for arsenic and
624 nitrate removal. Water Res. 38, 2053-2062.

625 Lagergren, S., 1898. Zur theorie der sogenannten adsorption geloster stoffe. Kungliga
626 svenska vetenskapsakademiens.Handlingar 24, 1-39.

627 Langmuir, I., 1918. The adsorption of gases on plane surfaces of glass, mica and
628 platinum. J. Am. Chem. Soc. 40, 1361-1403.

629 Li, M., Zhang, Z., Li, R., Wang, J.J., Ali, A., 2016. Removal of Pb (II) and Cd (II) ions
630 from aqueous solution by thiosemicarbazide modified chitosan. Int. J. Biol. Macromol.
631 86, 876-884.

632 Liang, X., Hart, C., Pang, Q., Garsuch, A., Weiss, T., Nazar, L.F., 2015. A highly
633 efficient polysulfide mediator for lithium–sulfur batteries. Nature communications 6,
634 5682.

635 Lindberg, B., Hamrin, K., Johansson, G., Gelius, U., Fahlman, A., Nordling, C.,
636 Siegbahn, K., 1970. Molecular spectroscopy by means of ESCA II. Sulfur compounds.
637 Correlation of electron binding energy with structure. Phys. Scripta 1, 286.

638 Manning, B.A., Goldberg, S., 1997. Adsorption and stability of arsenic (III) at the clay
639 mineral− water interface. Environ. Sci. Technol. 31, 2005-2011.

640 Monier, M., Akl, M., Ali, W., 2014. Preparation and characterization of selective phenyl
641 thiosemicarbazide modified Au (III) ion-imprinted cellulosic cotton fibers. J Appl
642 Polym Sci 131.

643 Navarro, R.R., Sumi, K., Fujii, N., Matsumura, M., 1996. Mercury removal from
644 wastewater using porous cellulose carrier modified with polyethyleneimine. Water Res.
645 30, 2488-2494.

646 Nieboer, E., McBryde, W., 1973. Free-energy relationships in coordination chemistry.
647 III. A comprehensive index to complex stability. Canadian Journal of Chemistry 51,
648 2512-2524.

649 Parsons, J.G., Dokken, K.M., McClure, J., Gardea-Torresdey, J.L., 2013. FTIR, XAS,
650 and XRD study of cadmium complexes with l-cysteine. Polyhedron 56, 237-242.

651 Pauling, L., 1967. The Nature of the Chemical Bond. the Chemical Bond. A Brief
652 Introduction to Modern Structural Chemistry.(A Shortened Version of the Nature of the
653 Chemical Bond.). Ithaca; Oxford University Press: London.

654 Phillips, C., 1965. RJP Williams Inorganic Chemistry, Vol. 1.

655 Qin, X., Zhou, J., Huang, A., Guan, J., Zhang, Q., Huang, Z., Hu, H., Zhang, Y., Yang,
656 M., Wu, J., 2016. A green technology for the synthesis of cellulose succinate for efficient
657 adsorption of Cd (II) and Pb (II) ions. RSC Advances 6, 26817-26825.

658 Redlich, O., Peterson, D.L., 1959. A useful adsorption isotherm. J. Phys. Chem. 63,
659 1024-1024.

660 Singha, A., Guleria, A., 2014. Chemical modification of cellulosic biopolymer and its
661 use in removal of heavy metal ions from wastewater. Int. J. Biol. Macromol. 67, 409-
662 417.

663 Sips, R., 1948. On the structure of a catalyst surface. J. Chem. Phys. 16, 490-495.

664 Stefaniu, C., Zaffalon, P., Carmine, A., Verolet, Q., Fernandez, S., Wesolowski, T.A.,
665 Brezesinski, G., Zumbuehl, A., 2015. Rigid urea and self-healing thiourea ethanolamine
666 monolayers. Langmuir 31, 1296-1302.

667 Tangsir, S., Hafshejani, L.D., Lähde, A., Maljanen, M., Hooshmand, A., Naseri, A.A.,
668 Moazed, H., Jokiniemi, J., Bhatnagar, A., 2016. Water defluoridation using Al 2 O 3
669 nanoparticles synthesized by flame spray pyrolysis (FSP) method. Chem. Eng. J. 288,
670 198-206.

671 Ucun, H., Bayhana, Y.K., Kaya, Y., Cakici, A., Algur, O.F., 2003. Biosorption of lead
672 (II) from aqueous solution by cone biomass of Pinus sylvestris. Desalination 154, 233-
673 238.

674 Wang, Z., Shen, D., Shen, F., Wu, C., Gu, S., 2017. Equilibrium, kinetics and
675 thermodynamics of cadmium ions (Cd2) removal from aqueous solution using

676 earthworm manure-derived carbon materials. Journal of Molecular Liquids 241, 612-
677 621.

678 Weber, T. W., Chakravorti, Ranjit K., 1974. Pore and solid diffusion models for
679 fixed-bed adsorbers. AIChE J., Wiley Online Library 20, 2, 228-238.

680 Weber, W., Morris, J., 1963. Intraparticle diffusion during the sorption of surfactants
681 onto activated carbon. J.Sanit.Eng.Div.Am.Soc.Civ.Eng 89, 53-61.

682 WHO, G., 2011. Guidelines for drinking-water quality. World Health Organization 216,
683 303-304.

684 Wilson, H., Tarbell, D., 1950. The action of aluminum bromide on some halogenated
685 thiophenols and benzyl phenyl sulfides. J. Am. Chem. Soc. 72, 5200-5205.

686 World Health Organization, 2008. Guidelines for drinking-water quality [electronic
687 resource]: incorporating 1st and 2nd addenda, vol. 1, Recommendations.

688 Xu, X., Gao, B., Tan, X., Yue, Q., Zhong, Q., Li, Q., 2011. Characteristics of amine-
689 crosslinked wheat straw and its adsorption mechanisms for phosphate and chromium
690 (VI) removal from aqueous solution. Carbohydr. Polym. 84, 1054-1060.

691 Yu, X., Tong, S., Ge, M., Zuo, J., Cao, C., Song, W., 2013. One-step synthesis of
692 magnetic composites of cellulose@ iron oxide nanoparticles for arsenic removal.
693 Journal of Materials Chemistry A 1, 959-965.
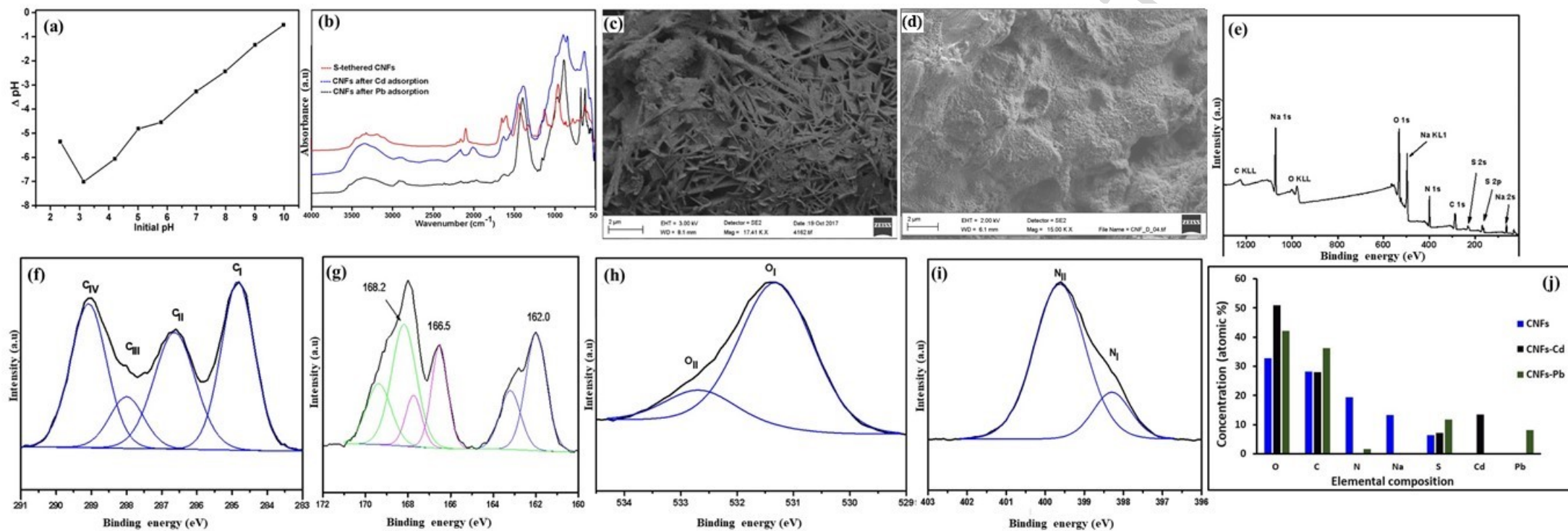
694

FIGURES

Fig. 1. (a) pH$_{PZC}$ measurements, (b) FT-IR spectra, (c, d) SEM images at different magnifications, XPS spectra of CNFs: (e) wide scan, (f) C1s, (g) S 2p, (h) O 1s, (i) N 1s, and (j) elemental composition of synthesized S-tethered CNFs.
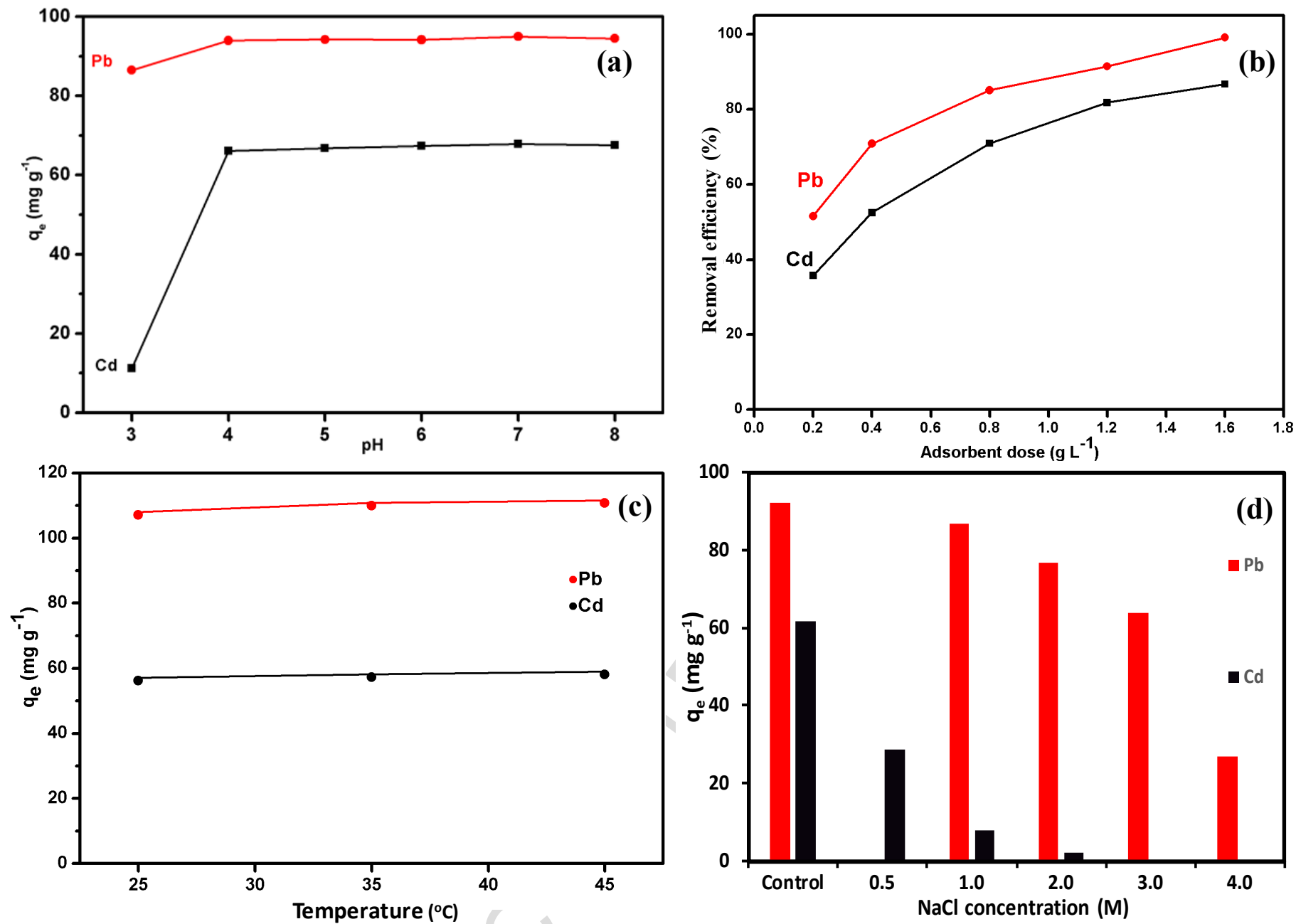
Fig. 2. Effect of (a) pH, (b) adsorbent dosages, (c) temperature, (d) ionic strength on adsorption of Pb(II) and Cd(II) by CNFs (metal ions concentration: 50 mg L^{-1}, CNFs dose: 0.5 g L^{-1}).
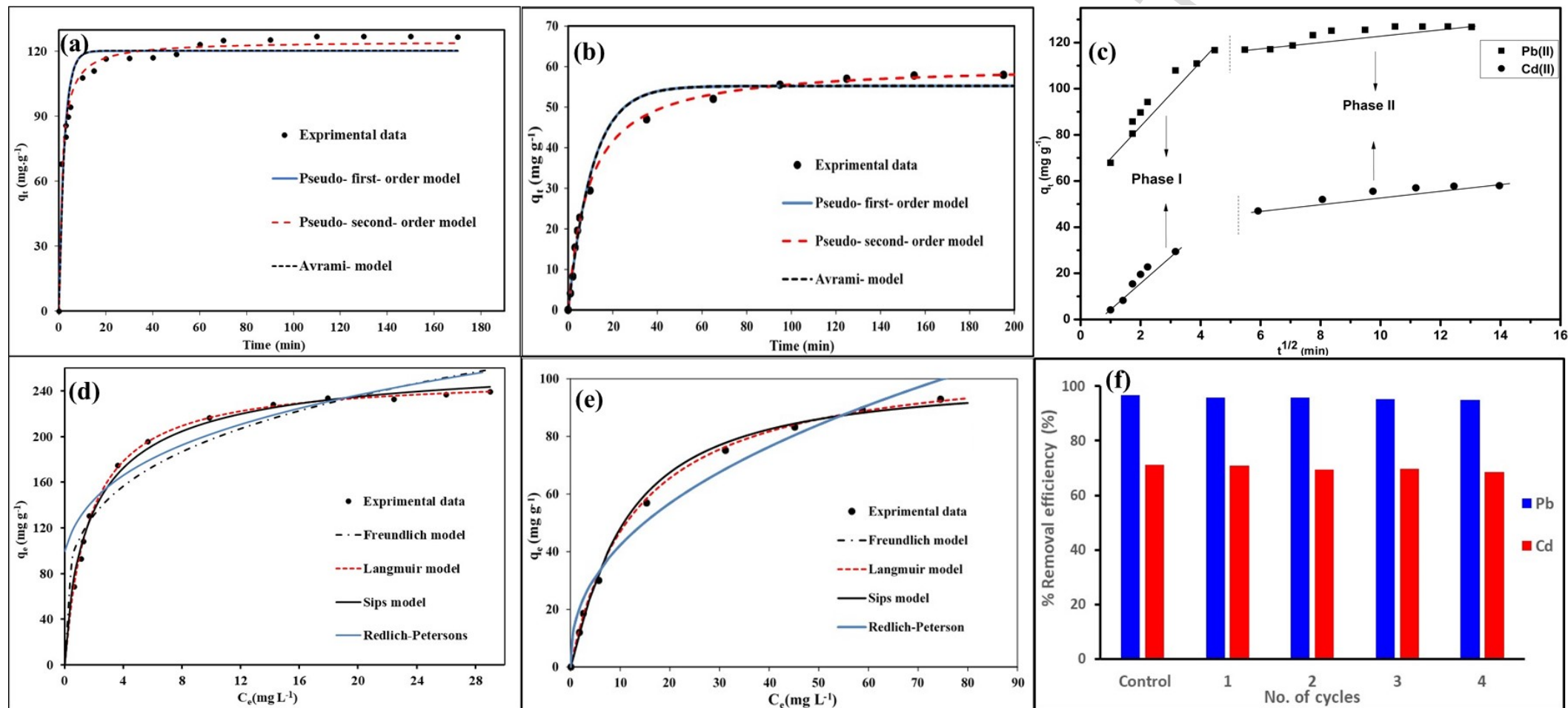
Fig. 3. (a, b) Pb(II) and Cd(II) adsorption kinetics modelling, (c) intra-particle diffusion modelling (metal ions concentration: 50 mg L^{-1}, CNFs dose: 0.5 g L^{-1}); (d, e) Pb(II) and Cd(II) adsorption isotherms modelling (metal ions concentration: C_i: 10 – 200 mg L^{-1} CNFs dose: 0.5 g L^{-1}), (f) regeneration studies of Pb(II) and Cd(II) adsorption by synthesized CNFs using 0.1 M NaOH as eluent.
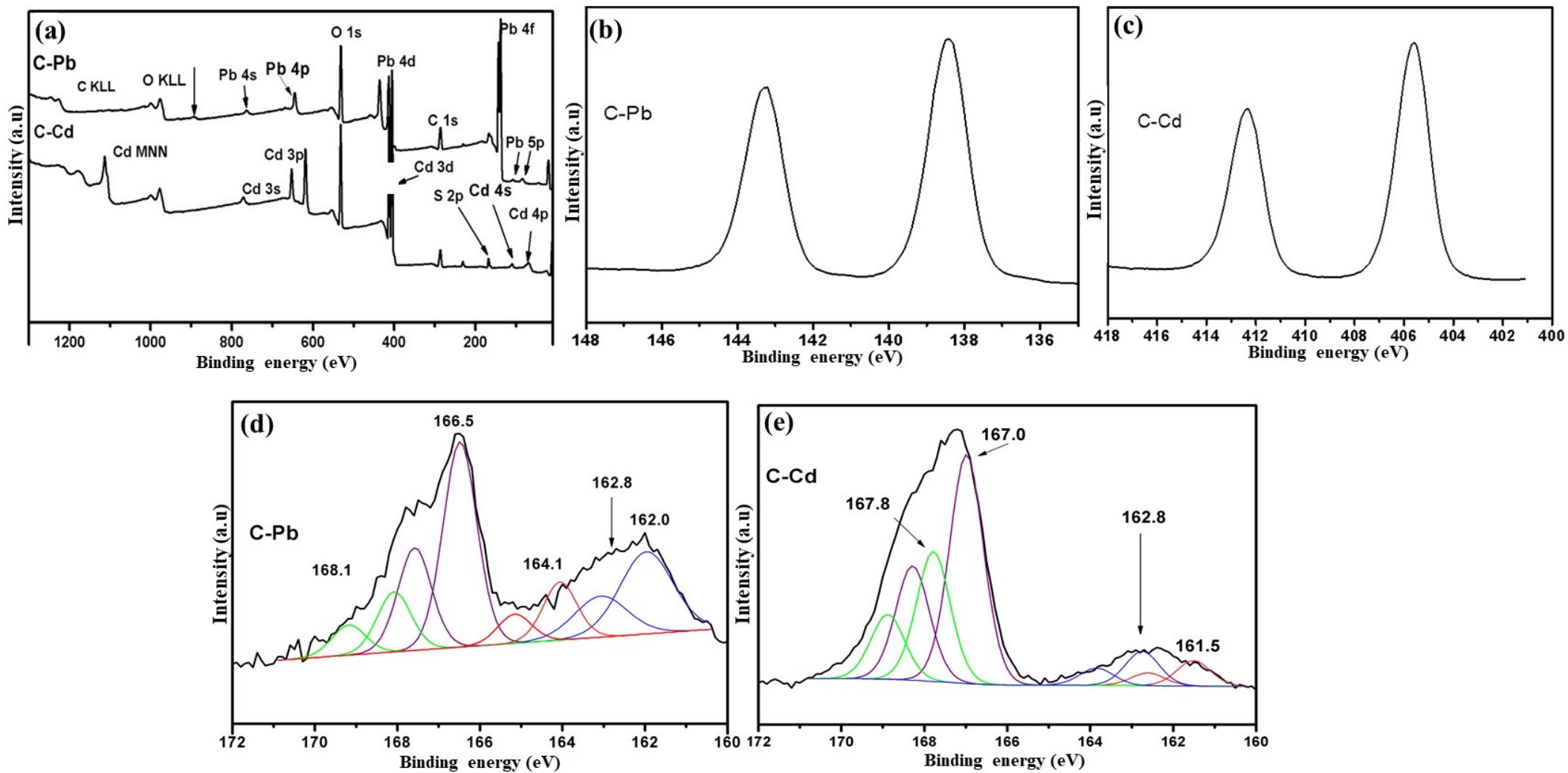
Fig. 4. (a) XPS wide scan spectrum of Pb(II) and Cd(II), (b, c) high resolution spectra of Pb(II) 4f and Cd(II) 3d, (d, e) S 2p spectra of Pb(II) and Cd(II) after adsorption onto CNFs.
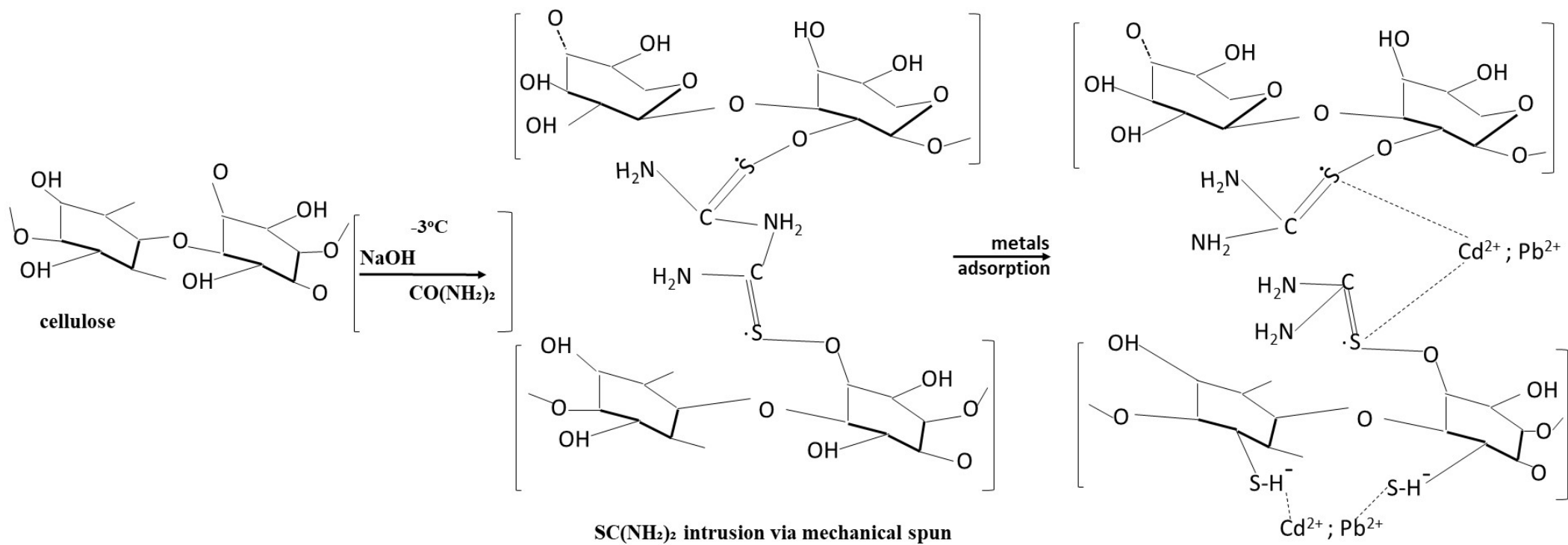
Fig. 5. Proposed mechanism of polymerization disruption and tethering of sulphur complexes on the disrupted cellulose chain and adsorption mechanism of metal ions.

Highlights:

(1) S-ligand tethered cellulose nanofibers were synthesized for metals adsorption.
(2) Adsorption capacity of S-CNFs was 1.16 mmol g^{-1} for Pb and 0.82 mmol g^{-1} for Cd.
(3) Ligand exchange is suggested as possible mechanism for both metal ions.
(4) Reusability studies revealed that synthesized adsorbent is resilient.
(5) Synthesized CNFs can be effectively used in industrial wastewater treatment.

TABLES

Table 1. Thermodynamic parameters of the adsorption of Pb(II) and Cd(II) by CNFs.

Temperature (°C)	Temperature (K)	$\Delta G°$ (kJ mol^{-1})		$\Delta H°$ (kJ mol^{-1})		$\Delta S°$ (kJ mol^{-1} K^{-1})	
		Pb(II)	Cd(II)	Pb(II)	Cd(II)	Pb(II)	Cd(II)
25	298.15	− 34.29	− 23.95	253.10	3.03	0.88	0.02
35	308.15	− 41.87	− 24.87				
45	318.15	− 53.61	− 25.76				

Table 2. Adsorption kinetics and isotherm parameters of Pb(II) and Cd(II) adsorption by synthesized CNFs.

Kinetic model	Parameter	Metal ion		Isotherm model	Parameter	Metal ion	
		Pb(II)	Cd(II)			Pb(II)	Cd(II)
Pseudo-first order	$q_{e\ exp}$ (mg g^{-1})	126.74	57.96	Langmuir	q_{exp} (mg g^{-1})	239.41	92.90
	$q_{e\ cal}$ (mg g^{-1})	120.23	55.22		q_{cal} (mg g^{-1})	239.64	92.32
	k_1 (min^{-1})	0.41	0.09		K_L (L mg^{-1})	0.24	0.08
	RMSE	13.23	3.48		RMSE	3.90	1.52
	R^2	0.959	0.984		R^2	0.999	0.999
					R_L	0.37	0.59
Pseudo-second order	$q_{e\ exp}$ (mg g^{-1})	126.74	57.96	Freundlich	K_F (mg g^{-1})	110.34	15.79
	$q_{e\ cal}$ (mg g^{-1})	123.78	57.97		n	3.95	2.34
	k_2 (g mg^{-1} min^{-1})	0.01	0.00		RMSE	23.90	6.01
	RMSE	6.91	1.64		R^2	0.984	0.988
	R^2	0.986	0.995				
Avrami	$q_{e\ exp}$ (mg g^{-1})	126.74	57.96	Sips	q_{exp} (mg g^{-1})	239.41	92.90
	$q_{e\ cal}$ (mg g^{-1})	120.23	55.21		K_s (L mg^{-1})	0.57	0.06
	k_{av} (g mg^{-1} min^{-1})	0.43	0.03		ns	1.23	0.87
	RMSE	13.23	3.47		RMSE	7.69	2.20
	R^2	0.959	0.989		R^2	0.998	0.979
Intra-particle diffusion	$q_{e\ exp}$ (mg g^{-1})	126.74	57.96	Redlich-Peterson	K_{RP} (L mg^{-1})	116.09	207.90
	K_p (g mg^{-1} min$^{-1/2}$)	3.43	4.08		q_{PR} (mg g^{-1})	51.66	39.76
	C (mg g^{-1})	64.47	11.38		RMSE	19.62	6.01
	RMSE	13.03	2.73		R^2	0.988	0.985
	R^2	0.897	0.897				

Table 3. Binding strength characterization parameters.

	Cd(II)	Pb(II)
z (charge)	2	2
R_{cryst}[a] (Å)	0.95	1.19
R_{hyd}[b] (Å)	4.26	4.01
X_m[c]	1.70	1.80
z^2/r_{cryst}[d1] (1/Å)	4.21	3.36
z^2/r_{hyd}[d2] (1/Å)	0.94	1.00
$X_m^2(r_{cryst}+0.85)$[e] (Å)	5.20	6.61
ΔX_m[f]	1.80	1.70
$1-exp(-\Delta X_m^2/4)$[g]	0.56	0.51
ξ[h] $= z^2/r_{hyd}/1-exp(-\Delta X_m^2/4)$ (1/Å)	1.69	1.94

[a] Shannon crystal radii (Evans, 1995)
[b] Nightingale hydrated ion radii(Kertes and Marcus, 1969)
[c] Pauling electronegativity (Dean, 1990)
[d] Parameter for hydration ([1]) or ionic bonding ([2]) strength(Phillips, 1965)
[e] Parameter for covalent bond character (0.85 is an appropriate constant assumed to reflect the radius of O and N donor atoms) (Nieboer and McBryde, 1973)
[f] Parameter for ionic bond character (Electronegativity of the metal relatively to oxygen)
[g] Fraction of ionic bond character (Pauling, 1967)
[h] Parameter for total binding strength.

Table 4. Adsorption capacity and removal efficiency of synthesized CNFs for different concentrations of metal ions from metal coating and mining seep wastewater.

	Metal coating wastewater				Mining seep wastewater			
Metal	Before adsorption (mg L^{-1})	After adsorption (mg L^{-1})	Adsorption capacity (mg g^{-1})	Removal efficiency **(%)**	Metal	Before adsorption (mg L^{-1})	After adsorption (mg L^{-1})	Uptake capacity (mg g^{-1})	Removal efficiency **(%)**
Pb	250*	2.73	504.14	98.92	Pb	230*	5.01	452.62	98.22
	310*	6.02	611.35	98.06		340*	9.99	667.43	97.22
	490*	46.44	889.71	90.54		420*	37.75	779.30	91.16
Cd	200*	135.88	133.44	32.84	Cd	192*	107.21	170.58	44.30
	310*	202.70	232.80	36.53		300*	227.20	158.04	25.84
	400*	275.40	244.84	30.77		400*	336.20	121.80	16.33
Zn	12.43	0.56	23.73	95.46	Zn	4.03	0.04	7.94	98.53
Hg	1.02	0.02	2.00	98.31	Ba	5.33	0.09	10.50	98.52
Mn	2.18	0.03	4.28	98.32	Mn		1.80	4.36	52.71
Ni	2.27	0.07	4.40	96.78					
Co	2.66	0.13	5.05	94.89					

(*Spiked concentrations)